ARTICLE

Electronic and Optical Properties of O-Terminated Armchair Graphene Nanoribbons

Dao-bang Lu[a,b], Chang-geng Luo[a], Yu-ling Song[a*], Qun-na Pan[c], Chun-ying Pu[a]

a. College of Physics and Electronic Engineering, Nanyang Normal University, Nanyang 473061, China
b. Henan Engineering Laboratory of Petroleum Equipment Intelligent Control, Nanyang 473061, China
c. Computer and Information Technology, Nanyang Normal University, Nanyang 473061, China

(Dated: Received on June 16, 2015; Accepted on September 16, 2015)

The structure, electromagnetic and optical properties of the O-terminated graphene nanoribbons with armchair edge are studied using first-principles theory. The results show that the O-terminated armchair edge are more stable than the H-terminated ribbons and show metallic character. Spin-polarized calculations reveal that the antiferromagnetic state are more stable than the ferromagnetic state. The energy band and density of states analyses show that the O-terminated armchair edge are antiferromagnetic semiconductors. Because of the terminated O atoms, the dielectric function has an evident red shift and the first peak is the strongest with its main contribution derived from the highest valence band. The peaks of the dielectric function, reflection, absorption, energy loss are related to the transition of electrons. Our results suggest that the O-terminated graphene nanoribbons have potential applications in nanoelectronics, opto-electric devices.

Key words: First-principles, Electronic properties, Optical properties, O termination, Graphene nanoribbons

I. INTRODUCTION

With the development of the nanotechnology, low-dimensional nanomaterials, especially nanoribbons, play a critical role in the fundamental research and potential microelectronic devices. As an important character, optical properties of the nanomaterial have been studied in detail during the past decades due to the rapid development of the first-principles calculation [1−5]. Since its experimental realization, graphene nanoribbons (GNRs) have become the subject of intensive research because of their exciting applications in several fields like optics, electronics, opto-electronics, spintronics, electron transport, and so on [6−13]. Usually, a carbon atom on the nanoribbon edge is terminated by H atom which is used to be a termination. Son *et al.* studied the energy gaps in the GNRs with H-terminated armchair or zigzag shaped edges and found that both always had direct nonzero band gaps [14]. Kawai *et al.* studied the GNRs both with and without H terminations intensively using first-principles calculations [15], and found that strong edge reconstruction occurred and thus the band structures, the dangling bonds changed the band gap of the armchair GNRs (AGNRs). Edge states of the GNRs influence edge stress as well as edge energies of the ribbons [16], and hydrogen termination results in stress-free state for both zigzag and armchair edges.

Since many of the unique properties of the GNRs are associated with edge states, different atoms termination in the edges can significantly alter the electronic properties of the ribbons. Therefore, it is essential to gain better understanding of the influence of edge termination on the electronic properties of GNRs. Besides H atom, the GNRs terminated with F atoms have also been investigated. Theoretical studies for the GNRs show that the electronic properties of the GNRs can be modulated by the terminated F atoms [17], the band gaps of AGNRs are smaller than those of the H-terminated AGNRs because of the σ-π mixing effect.

Recently, there have been several theoretical studies concerning edge-oxidized (O) zigzag GNRs [8, 9]. It is predicted that, compared to H terminated GNRs, the oxidized ribbons are more stable except for the etheric groups and show metallic band structures caused by the larger electronegativity of oxygen relative to carbon. The changes of the AGNRs' electronic structures caused by the terminated O atoms would influence the optical properties. At present, great evolvements of relative theoretical and experimental researches about the optical properties of the AGNRs and chiral AGNRs with H atoms termination have been obtained in scientific research field [18−20]. Up to now, there are no reports about the electronic and optical properties of the armchair O-terminated GNRs.

*Author to whom correspondence should be addressed. E-mail: yuling985@163.com, Tel.: +86-377-63513563

In this work, relative stability, the structural, electromagnetic and optical properties of the O-terminated AGNRs have been investigated by using the first-principles. The energy band structures, the density of states (DOS), and the optical properties of the systems are also analyzed.

II. MODEL AND CALCULATION METHOD

The calculations are performed using the Vienna *ab initio* simulation package (VASP) based on DFT [21−24]. The electron-ionic core interaction is represented by the projector augmented wave (PAW) potentials [25] which are more accurate than the ultra-soft pseudopotentials. To treat electron exchange and correlation, we chose the Perdew-Burke-Ernzerhof (PBE) [26] formulation of the generalized gradient approximation (GGA), which yields the correct ground state structure of the combined systems. A conjugate-gradient algorithm is used to relax the ions into their ground states, and the energies and the forces on each ion are converged within 1.0×10^{-4} eV/atom and 0.02 eV/Å, respectively. The cutoff energy for the plane-waves is chosen to be 450 eV. The O $3s^2 3p^4$, C $2s^2 2p^2$, and H $1s^1$ electrons are treated as valence electrons. In order to simulate infinite long isolated nanoribbon, we use a super-cell geometry where each plane is separated from its replica by 15 Å in both edge-to-edge and layer-to-layer directions. This interval is enough to ensure negligible interaction between the ribbon and its periodic images because the identical results are obtained for larger separation distances. The k-point is sampled according to the Monkhorst-Pack automatic generation scheme with their origin at Γ point, together with a Gaussian smearing broadening of 0.2 eV. We investigate for infinitely long single-layer AGNRs and set the periodicity of the AGNRs along the ribbon axis.

A hexagonal network of the AGNRs was adopted. The width of the AGNR is defined by the number of the C−C dimer lines (N_a) across the ribbon width. Thus we refer an AGNRs with N_a dimer lines as N_a-AGNRs. As an example, the geometry structure of the 13-AGNR terminated with O atoms is shown in Fig.1. The brown and red balls represent C and O atoms, respectively.

III. RESULTS AND DISCUSSION

We investigated the O-terminated AGNRs with the width N_a=3−19. According to our calculation method, we also calculate the H-terminated AGNRs with the same width. Comparing the total energy of the H- and O-terminated 19-AGNR, we find the H-terminated 19-AGNR has higher total energy of 6.10 eV/cell than the O-terminated 19-AGNR, showing the O-terminated 19-AGNR is more stable.

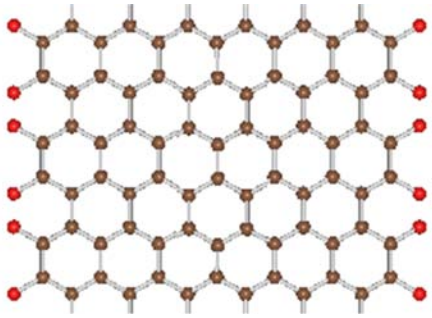

FIG. 1 The geometry structure of 13-AGNR with O atoms termination. The brown and red balls represent C and O atoms, respectively.

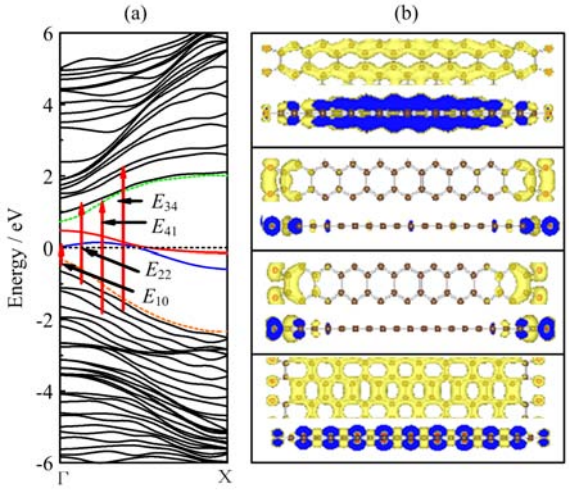

FIG. 2 (a) The band structure of the O-terminated 19-AGNR. The Fermi level is set to zero and indicated by the black dashed line. (b) The charge density isosurfaces (from top to bottom panels for the green dashed, red solid, blue solid and orange dash dotted lines) as well as their sections (the bottom panels in each rectangular boxes) of selected bands for N_a=19.

As an example, the band structures of the O-terminated 19-AGNR as well as the charge density isosurfaces and their sections of selected bands (from the top to down panels for the red, green and blue bands) are shown in Fig.2, where all the O-terminated AGNRs yield the same band structure. To compare the influence of the O and H atoms on the energy band structures, in Fig.3, we also give the energy band structures with N_a=19 as well as the charge density isosurfaces and their sections of selected bands (the lowest unoccupied conduction band (LUCB), the highest occupied valence band (HOVB)) and the red dashed band of the H-terminated AGNR.

For the H-terminated 19-AGNR, the LUCB and the HOVB appearing at Γ point are separated representing a direct semiconductor character, which are in good agreement with existing experimental data in Ref.[4]. In Fig.3, the top and the middle panels indicate that

DOI:10.1063/1674-0068/29/cjcp1506125

the charge density of the LUCB comes mainly from the zigzag C−C chains across the ribbon width and the σ electrons, while for that of the HOVB, it comes mainly from the C−C dimer lines across the ribbon width and the π electrons, and the bottom panel shows the red dashed band main from the σ electrons which also contains the C−H sp^2 hybridinzation electrons.

For the O-terminated 19-AGNR, from Fig.2, it can be seen that the band structures are very similar to that of the H-terminated 19-AGNR shown in Fig.3. Moreover, the LUCB (the green dashed line) and the HOVB (the orange dash dotted line) move upward and downward and two extra half filled bands (the red and blue solid lines) across the Fermi level, which yields a metallic band structure. The charge density isosurfaces as well as their sections corresponding to the LUCB, HOVB, and the two half filled bands can help us gain deep insight into the contributions of these bands near the Fermi level.

In Fig.2(b), the top and the bottom panels indicate that the charge density of the LUCB comes mainly from the zigzag C−C chains across the ribbon width and the σ electrons, while for that of the HOVB comes mainly from the C−C dimer lines across the ribbon width and the π electrons, the situation is similar to that of the H-terminated 19-AGNR shown in Fig.3(b). On the other hand, the contribution to the charge density of both LUCB and HOVB from the π electrons of the O atoms can't be ignored. In Fig.2(b), the middle two panels indicate that the charge density of the two half filled bands are all contributed from the edge C atoms and the O atoms. The difference is the charge density of the red band comes mainly from the σ electrons of the edge C atoms while that of the blue one comes mainly from the π electrons of the edge C atoms.

We show the total density of states (DOS), projected density of states (PDOS) onto the O atom and one of the edge C atom in Fig.4 (a), (b), and (c) to illustrate the metallic band structure, respectively, for 19-AGNR with O termination as one example. As predicted from the energy band structures of the O- and H-terminated 19-AGNRs above, it can be clearly seen in Fig.4(a) that a peak appears at the Fermi level E_F, while there is not a peak in Fig.4 (d)−(f), which is the total DOS, PDOS onto the O atom and one of the edge C atom for 19-AGNR with H termination. Comparing Fig.4 (b) and (c), we find that this DOS peak comes from the edge C atom and the O atom especially its p orbital electrons.

For the O-terminated 19-AGNR, the two single occupied 2p orbitals of the O atom are expected to form one σ and one π bond with the edge C atom. Accordingly, the π orbits of the edge C atom will be terminated. For the H-terminated 19-AGNR, each edge C atom is terminated by a single H atom for sp^2 hybridization and forms one σ bond. These results can be clearly seen from the charge density isosurfaces as well as their sections of selected bands for 19-AGNRs with O and H termination. Therefore, in Fig.4 (b) and (c) within the

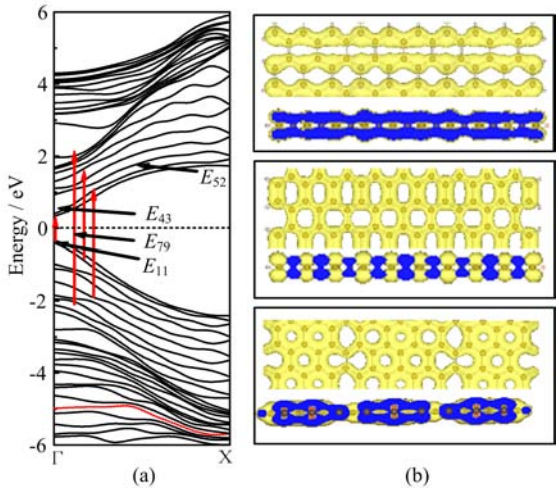

FIG. 3 (a) The band structure of the 19-AGNR with H termination. The Fermi level is set to zero and indicated by the black dashed lines. (b) The charge density isosurfaces as well as their sections of selected bands for the LUCB (top panel), the HOVB (middle bottom panel) and the red dashed band (bottom panel) of the N_a=19.

scope of −2.5<energy<0 eV, the O-p and C-p show a strong hybridization. Instead, in Fig.4 (e) and (f) near the −5 eV, the H-s and C-p show a strong hybridization.

Now, we perform a spin-polarized DFT calculation for the AGNRs with O termination at both edges. As an example, Fig.5 shows the band structures, DOS, and the difference charge density (ρ^{up}-ρ^{down}) of the 19-AGNR with O termination in both ferromagnetic and antiferromagnetic states.

We find a ferromagnetic excited state with slightly higher energy of 0.19 eV/cell above the antiferromagnetic ground state for the O terminated 19-AGNR. So, compared with the nonmagnetic semiconductor of the H-terminated 19-AGNR, in its ground state, the O terminated 19-AGNR is indirect semiconducting, while the excited states is metallic. In the antiferromagnetic ground state, the bands for both spins are degenerate and induce a magnetic moment of 0 μ_B and thus leading to a symmetrical DOS in Fig.5(b2), while for the ferromagnetic excited state O terminated 19-AGNR, the up-spin (red dashed lines) and down-spin (black solid lines) bands split from each other and induce a magnetic moment of 3.53 μ_B and thus leading to an asymmetrical DOS in Fig.5(b1).

The difference charge density ($\rho^{up}-\rho^{down}$) for the ferromagnetic excited state of the O terminated 19-AGNR plot in Fig.5(c1) indicates that the spin states at opposite edges have the same spin orientations and show decaying tails into the corresponding inner sublattices, while in Fig.5(c2) for the antiferromagnetic ground state, the spin states at opposite edges have different spin orientations.

As a comparison, our calculated charge densities of

DOI:10.1063/1674-0068/29/cjcp1506125

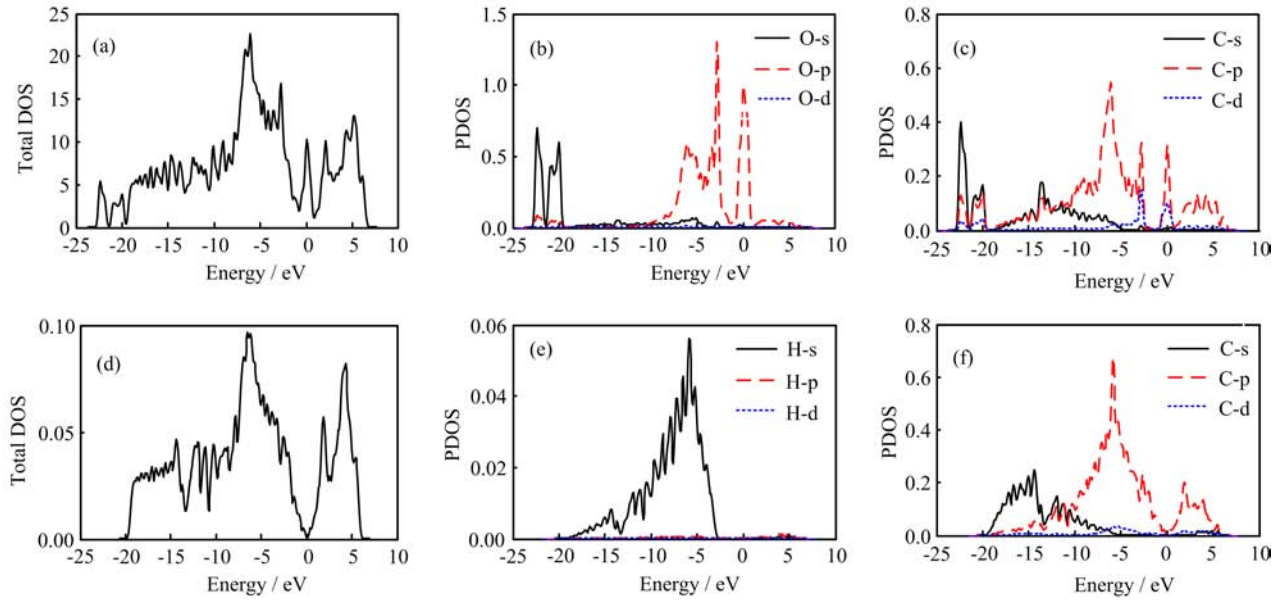

FIG. 4 (a) The DOS, (b) PDOS onto the O atoms and (c) one of the edge C atom of the O-terminated 19-ACNR as well as (d) the DOS, (e) PDOS onto the H atom and (f) one of the edge C atom of the H-terminated 19-ACNR. In PDOS, the black dotted, red and blue dashed lines are s, p, and d orbits, respectively.

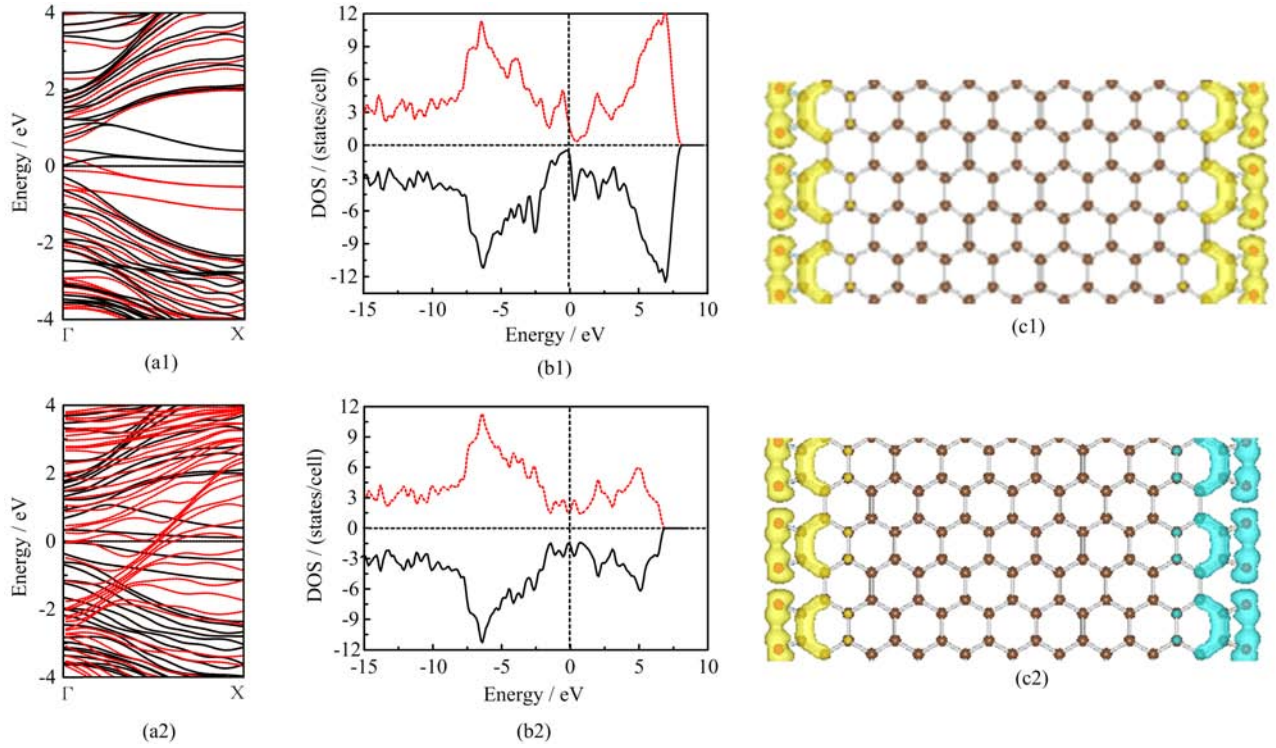

FIG. 5 The band structures (a), DOS (b) as well as the difference charge density ($\rho^{\mathrm{up}}-\rho^{\mathrm{down}}$) (c) of the O-terminated 19-AGNR in ferromagnetic (a1, b1, c1) and antiferromagnetic (a2, b2, c2) states. In (a) as well as (b), the red dashed and black solid lines represent the up-spin and down-spin, respectively, and the Fermi level is set to zero energy and indicated by black dashed lines. In top view of the difference charge density (c), the yellow and green isosurfaces corresponding positive (more up-spin) and negative (more down-spin) spins, respectively.

DOI:10.1063/1674-0068/29/cjcp1506125

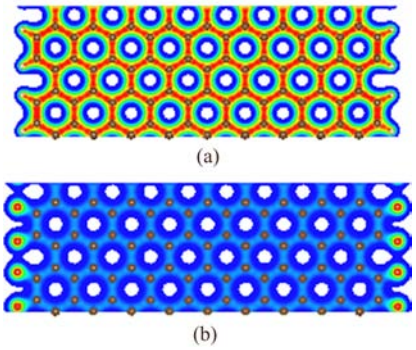

FIG. 6 The charge density contours of (a) H-terminated 19-AGNR and (b) O-terminated 19-AGNR.

the H- and O-terminated 19-AGNRs are given in Fig.6 (a) and (b), respectively. The maximum density value of the H-terminated 19-AGNR is 0.34 elections/Å^3 around H and C atoms while 1.22 elections/Å^3 for the O-terminated 19-AGNR around O atoms. Because the electronegativity of 3.5 for O atom is larger than that of 2.5 for C atom, the O atoms receive electrons and become negatively charged while C atoms donate electrons and become positively charged, which result in a typical ionic binding feature between the edge O atom and its nearest C atom. However, the C−H bonds in Fig.6(a) display a covalent bonding feature. This is because that the electronegativity of 2.5 for C atom and 2.1 for H atom has not much difference. The electrons distribute close to equal between the C and H atoms.

Dielectric function has more superiority than some macro optical constants, which can reflect the information between the band structure and optical spectra of solid materials, and also can get the better characterization of the physical properties.

The complex dielectric function $\varepsilon(\omega)=\varepsilon_1+i\varepsilon_2(\omega)$, where ε_1 is the real part and ε_2 is the imaginary part of the dielectric function, ε_2 can be obtained by solving the momentum matrix elements of the occupied states and unoccupied states. The imaginary and real parts of the H- and O-terminated 19-AGNRs are given in Fig.7 (a) and (b), respectively. It is shown that, firstly, the imaginary and real parts shapes of the O-terminated 19-AGNR with the change of the photon energy are similar to that of H-terminated ones. Secondly, the imaginary and real parts of the O-terminated 19-AGNR have an evident red shift, that is, the curves moves to the low frequency zone, which is mainly attributed to the energy band structure changing at the Fermi level because of the O atoms being added to the system. For instance, in Fig.7(a), the first four obvious peaks in the low frequency zone of the O-terminated 19-AGNR located at about 0.44, 1.96, 2.88, and 3.76 eV, and 0.63, 2.04, 3.02, and 3.93 eV for the H-terminated 19-AGNR. Combining with the band structure in Fig.2 and Fig.3, we used E_{mn} to mark the interband transitions from the mth valence band to the nth conduction band, counted from

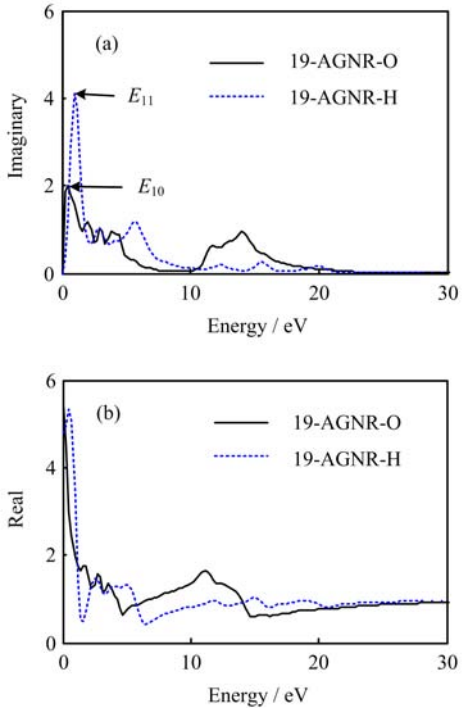

FIG. 7 Dielectric function of H- and O-terminated 19-AGNRs. (a) Imaginary part and (b) real part.

the Fermi level as indicated by the red arrows. For example, the aforementioned first four dielectric peaks of the O-terminated 19-AGNR located at about 0.44, 1.96, 2.88, and 3.76 eV are formed with the optical transitions of E_{10}, E_{22}, E_{41}, and E_{34} at each location of the red arrows (where E_{10} denotes the interband transitions from the highest valence band to the blue energy band which crosses the Fermi level), respectively, and for the H-terminated 19-AGNR, the first four dielectric peaks originated form E_{11}, E_{43}, E_{52}, and E_{79}. The first peak, in H- and O-terminated 19-AGNRs cases, is the strongest with its main contribution derived from the highest valence band, and the it can also be seen from Fig.7(a) that the imaginary part of the dielectric functions goes to zero for both H- and O-terminated 19-AGNRs in the high energy range. These properties indicate that different terminated atoms of AGNRs affect mainly the optical properties in the low energy range. Figure 7(b) shows the real parts of dielectric functions of H- and O-terminated 19-AGNRs have the basically same change trends as the imaginary parts in the low energy area.

In order to determine the origination of the dielectric peaks, as examples, we calculated the charge density distribution corresponding to the E_{10} and E_{11} as shown in Fig.8. From Fig.8, it can be seen that the charge density distribution are changed obviously. It is because the O atoms make the important contribution to the charge density distribution. Especially, the electrons of the O atoms prompt the visible change in the imaginary

DOI:10.1063/1674-0068/29/cjcp1506125

part of the dielectric function.

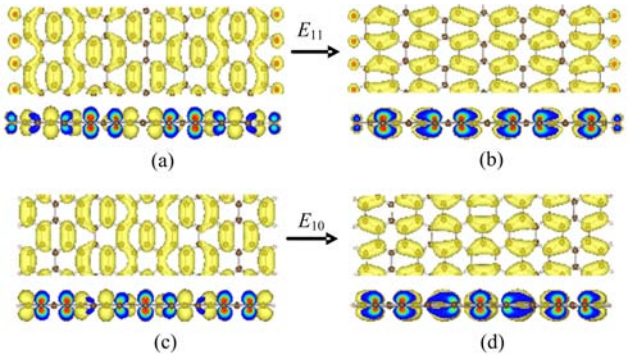

FIG. 8 The charge density isosurfaces (top panels) as well as their sections (bottom panels) corresponding to the E_{10} of O-terminated 19-AGNR. (a) The orange energy band and (b) the blue energy band at Γ point in Fig.2, as well as the E_{11} of H-terminated 19-AGNR (c) the HOVB and (d) the LUCB at Γ point in Fig.3.

Figure 9 shows the reflectivity, absorption coefficient and the energy loss function of H- and O-terminated 19-AGNRs in the energy range of 0−30 eV, respectively.

In Fig.9(a), there are several peaks in the low energy range and these peaks correspond to that of the dielectric function in Fig.7, which indicates that both of H- and O-terminated 19-AGNRs have the same transition mechanism. The high energy area is characterized by zero reflectivity. That is to say, in the high energy range, the systems can be seen as optically transparent materials. Figure 9(b) presents the absorption coefficient of the H- and O-terminated 19-AGNRs. It can be seen that the main absorption region still locates at the low energy area 0−25 eV. In the high energy area, the absorption coefficient is almost zero. In Fig.9(c), the energy loss peaks are consistent with the trailing edges in the reflection spectra [2]. For instance, the energy loss peaks of the O-terminated 19-AGNRs are at about 1.11, 2.21, 3.10, 4.65, and 14.8 eV corresponding to the abrupt reduction of reflection. These peaks represent the properties related to the plasma resonance, which is corresponding to the plasma frequency.

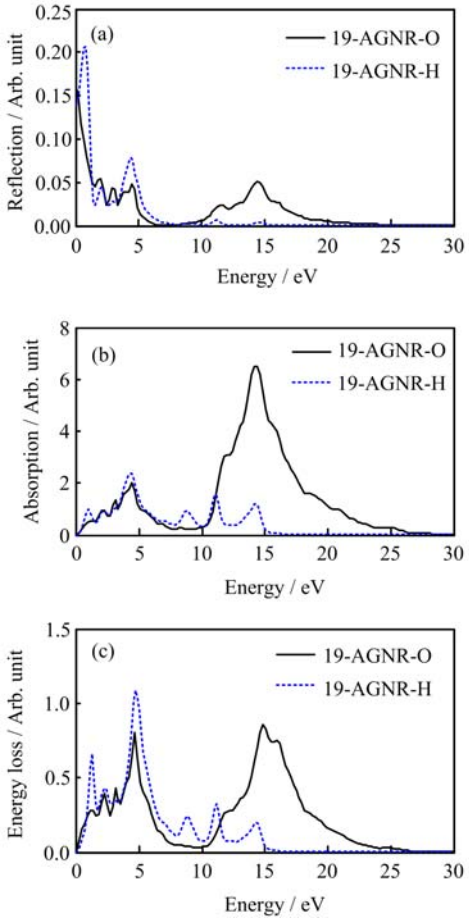

FIG. 9 (a) Reflection, (b) absorption, and (c) energy loss spectra of H- and O-terminated 19-AGNRs.

IV. CONCLUSION

In this work, the electronic, magnetic and optical properties of O-terminated AGNRs with different widths have been studied by using first-principles method under GGA. Several important findings are summarized as follows: (i) The energy band structures and properties of the O-terminated AGNRs are very different from that of the H-terminated one. The former are metallic, while the latter are semiconductor. (ii) The spin-polarized DFT calculation for the 19-AGNR reveals that the O terminated 19-AGNR is indirect semiconducting in its antiferromagnetic ground state, while the ferromagnetic excited state is metallic. (iii) The large asymmetry in charge distribution displays a typical ionic binding feature between the O atom and its nearest C atom, while C−H bond displays a typical covalent bonding feature. (iv) Research on the optical properties of the O-terminated 19-AGNR shows that, the dielectric function has an evident red shift and the first peak is the strongest with its main contribution derived from the highest valence band and the different terminated atoms of AGNRs affect mainly the optical properties in the low energy range.

The results show that different terminations can affect the electronic and magnetic properties of the AGNRs, which therefore can be tuned by using different terminations. Because of the rich electronic, magnetic and optical properties, we expect the potential applications of the O-terminated AGNR in electronics nanodevices.

V. ACKNOWLEDGMENTS

This work was supported by the Henan Joint Funds of the National Natural Science Founda-

DOI:10.1063/1674-0068/29/cjcp1506125

tion of China Natural Science Foundation of China (No.U1404608 and No.U1304612), the Science and Technology Key Projects of Henan Province, China (No.1502102210124), the Special Fund for Theoretical Science Foundation of Nanyang Normal University, China (No.ZX2013018), and the Henan Province Key Scientific Research project (No.16B510004).

[1] L. Y. Li, W. H. W, H. Liu, X. D. Liu, Q. G. Song, and S. W. Ren, J. Phys. Chem. C **113**, 8460 (2009).
[2] D. Allali, A. Bouhemadou, and S. Bin-Omran, Compt. Mater. Sci. **51**, 194 (2011).
[3] H. Nematian, M. Moradinasab, M. Pourfath, M Fathipour, and H. Kosina, J. Appl. Phys. **111**, 093512 (2012).
[4] Y. J. Du, B. K. Chang, H. G. Wang, J. J. Zhang, and M. S. Wang, Chin. Opt. Lett. **10**, 051601 (2012).
[5] F. L. Shyu, Physica B **452**, 7 (2014).
[6] S. Dutta, A. K. Manna, and S. K. Pati, Phys. Rev. Lett. **102**, 096601 (2009).
[7] F. Cervantes-Sodi, G. Csnyi, S. Piscanec, and A. C. Ferrari, Phys. Rev. B **77**, 165427 (2008).
[8] I. Silveiro, Juan Manuel Plaza Ortega, and F. Javier García de Abajo, Light Sci. Appl. **4**, e241 (2015).
[9] L. Yang, M. L. Cohen, and S. G. Louie, Nano Lett. **7**, 3112 (2007).
[10] P. Lu, Z. H. Zhang, and W. L. Guo, Phys. Lett. A **373**, 3354 (2009).
[11] M. Y. Han, J. C. Brant, and P. Kim, Phys. Rev. Lett. **104**, 056801 (2010).
[12] G. Lee and K. Cho, Phys. Rev. B **79**, 165440 (2009).
[13] V. A. Rigo, T. B. Martins, Antonio J. R. da Silva, A. Fazzio, and R. H. Miwa, Phys. Rev. B **79**, 075435 (2009).
[14] Y. W. Son, M. L. Cohen, and S. G. Louie, Phys. Rev. Lett. **97**, 216803 (2006).
[15] T. Kawai, Y. Miyamoto, O. Sugino, and Y. Koga, Phys. Rev. B **62**, 16349 (2000).
[16] S. Jun, Phys. Rev. B **78**, 075405 (2008).
[17] D. B. Lu, Y. L. Song, Z. X. Yang, and G. Q. Li, Appl. Surf. Sci. **256**, 6313 (2010).
[18] X. X. Peng, W. H. Liao, and G. H. Zhou, Chin. Phys. Lett. **25**, 3436 (2008).
[19] D. Prezzi, D. Varsano, A. Ruini, A. Marini, and E. Molinari, Phys. Rev. B **77**, 041404(R) (2008).
[20] M. Berahman1, M. Asad, M. Sanaee, and M. H. Sheikhi, Opt. Quant. Electron. **47**, 3289 (2015).
[21] G. Kresse and J. Hafner, Phys. Rev. B **47**, 558 (1993).
[22] G. Kresse and J. Hafner, Phys. Rev. B **49**, 14251 (1994).
[23] G. Kresse and J. Furthmüller, Comput. Mater. Sci. **6**, 15 (1996).
[24] G. Kresse and J. Furthmüller, Phys. Rev. B **54**, 11169 (1996).
[25] G. Kresse and D. Joubert, Phys. Rev. B **59**, 1758 (1999).
[26] J. P. Perdew, K. Burke, and M. Ernzerhof, Phys. Rev. Lett. **77**, 3865 (1996).

DOI:10.1063/1674-0068/29/cjcp1506125